PIER C

(Received 13 July 2026, Accepted 2 September 2026, Scheduled 22 September 2026)

Compact Frequency-Reconfigurable Diamond-Slotted Antenna for Wideband 5G/6G and IoT Applications

Salah E. El Aoud[1], Hind Abbaoui[2], Nasima El Assri[1], Saida Ibnyaich[1], Abdelouhab Zeroual[1], Mohd M. Ismail[3,*], Sharman Sundarajoo[4], and Ahmed J. A. Al-Gburi[5,*]

[1]*LISI Research Laboratory, I2SP Team, Department of Physics, Faculty of Sciences Semlalia Cadi Ayyad University, UCA, Marrakesh, Morocco*
[2]*LSEEET Research Laboratory, Department of Physics, Faculty of Sciences and Techniques Gueliz Cadi Ayyad University, UCA, Marrakesh, Morocco*
[3]*Fakulti Teknologi Dan Kejuruteraan Elektronik Dan Komputer (FTKEK), Universiti Teknikal Malaysia Melaka (UTeM) Jalan Hang Tuah Jaya, 76100, Durian Tunggal, Melaka, Malaysia*
[4]*School of Engineering, Asia Pacific University of Technology & Innovation, Kuala Lumpur, Malaysia*
[5]*Strategic Research Institute (SRI), Asia Pacific University, Jalan Teknologi 5 Taman Teknologi Malaysia, 57000, Kuala Lumpur, Malaysia*

ABSTRACT: This paper introduces an ultra-miniaturized, reconfigurable antenna for wireless communication applications. The suggested reconfigurable antenna is fabricated on an FR4-epoxy substrate ($20 \times 20 \times 1.6\,\text{mm}^3$, $\varepsilon_r = 4.4$), and it provides a miniature factor 79% which is an outstanding value. Frequency reconfiguration can be achieved using two PIN diodes, which make the proposed antenna capable of working in various frequencies, including 5G/6G, WLAN, HiperLAN, V2X, WiMAX, Wi-Fi 6E/7/8, and S/C/X/Ku bands. With the analysis performed by CST Studio Suite, the proposed antenna shows outstanding quantitative results without any sacrifice in its size, cost, or complexity. In this context, the antenna shows dual-band impedance bandwidths of 1.36 GHz and 6.4 GHz. Additionally, it has 2 dBi of peak gain and 79% high radiation efficiency.

1. INTRODUCTION

Rapid changes in wireless communication techniques, coupled with the development of new technological platforms, namely, Internet of Things (IoT) technology and vehicle-to-everything (V2X) communications, have led to the need for reliable, high-capacity, and adaptive wireless communication devices, which demand wireless systems equipped with ultra-broadband width, low latency, high reliability, and high data-rate capability [1, 2]. Thus, the importance of small, high-performance antennas becomes obvious in next-generation communication technologies [3–6]. It should be mentioned that antenna reconfiguration is accomplished by integrating different electronic switching elements, which include radio frequency (RF) PIN diodes, varactor diodes, and RF micro-electromechanical switches (MEMSs) [7–9].

The first of many advantages offered by frequency-reconfigurable antennas is small size, making them very suitable for devices in which the size is restricted. Additionally, frequency-reconfigurable antennas have stable radiation patterns throughout their entire spectrum of frequencies [10, 11]. Another critical function of frequency-reconfigurable antennas is that they minimize co-site interference and jamming susceptibility, making them an integral part of developing modern wireless communication systems [12–14].

Traditional wireless systems, such as fourth-generation Long-Term Evolution (4G LTE), are reaching their capacity levels in spectral efficiency and delay. In light of increasing demands on mobile data due to many emerging mobile devices, there is a need to come up with new communication technologies that can cater to future demands. The importance of such an innovative approach is more evident in urban areas and mission-critical applications requiring reliable and fast communication [7]. To address the identified problem, 5G mobile and wireless networks have been developed. 5G can be referred to as a revolution in communication technology due to its unique attributes, such as eMBB, URLLC, and mMTC. These attributes make 5G capable of supporting a variety of applications, including video streaming, virtual reality, and industrial automation [15]. The central aim of 5G technology is to offer smooth connectivity with better performance attributes, such as increased data rates, lower latency (down to even 1 ms), improved spectrum efficiency, and extensive heterogeneity support for networks. Additionally, 5G technology makes it possible to have pervasive communication between devices (device-to-device communication) and efficient allocation of spectrum in multiple bands. With such advantages, 5G is not just an enhanced version of its older counterparts, but it is the foundation upon which future digital transformation will happen in sectors such as healthcare, transport, industry, and smart cities [16–18].

* Corresponding authors: Mohd Muzafar Ismail (Muzafar@utem.edu.my); Ahmed Jamal Abdullah Al-Gburi (ahmedjamal@ieee.org).

doi:10.2528/PIERC26071302

Published by THE ELECTROMAGNETIC ACADEMY

Therefore, in the coming decade, the existing 5G infrastructure will face significant limitations regarding capacity and performance, emphasizing the necessity to develop a new generation of network technologies such as 6G. The World Radiocommunication Conference 2023 (WRC-23) has taken considerable steps in this regard by allocating the 6.425–7.125 GHz frequency range as an International Mobile Telecommunications (IMT) band. Additionally, the conference recommended allocating 7.125–8.4 GHz frequency range as an IMT band at the next WRC-27 meeting in 2027. Such decisions have become a crucial milestone toward implementing the new technology expected to be deployed around 2030. The huge bandwidth of 2 GHz in the upper mid-band frequency range will meet the needs of future 6G networks in extreme speed, low latency, and high connectivity. China officially granted the 6.425–7.125 GHz frequency range for 6G purposes in July 2023 [3].

These new bands of 6G and 5G attract researchers to develop antennas that can be useful in both applications during the transition period from 5G to 6G. This flexibility is possible with frequency-reconfigurable antenna designs for 5G and 6G [10, 19].

A vast number of different frequency-reconfigurable antenna design structures has been presented in the literature. For instance, a wide variety of antenna designs, including small-size, electronically-tunable slot antennas for high-frequency operations and differential antennas that can operate at one or multiple frequencies, are available [7, 20, 21]. In [22], a miniaturized flexible antenna based on a single PIN diode is proposed, operating across three frequency bands due to its frequency-reconfigurability properties. Ref. [23] presents a novel, highly adaptable multiband antenna, with an extremely small footprint of $25 \times 35 \times 0.254\,\text{mm}^3$. It has a frequency-tunable structure to meet diverse applications in wireless communication. Ref. [24] describes a dual-feed, dual PIN diode-based reversible stacked microstrip patch antenna that can be used for land mobile and satellite communications. Ref. [25] introduces a dual-band microstrip antenna with a hexagonal slot and single-feed configuration. Various types of planar and three-dimensional (3D) reconfigurable antennas have been reported in the literature and can be used for different applications, including wireless communication and radar communications [26]. Among the various designs, some have focused on operation in the L and X bands [27]. Design innovations keep coming, like in [26], where a novel reconfigurable antenna is designed for IoT application with a size of only $40 \times 40\,\text{mm}^2$. In the area of Multiple-Input Multiple-Output (MIMO) technique, reconfigurable antenna structures using dual printed dipole antennas and PIN diode switches were examined to provide increased adaptability via tuning both antenna patterns and operating frequencies [28, 29].

One of many techniques that allow frequency reconfigurability is the judicious application of ON/OFF switching conditions [30]. Varactor diodes, RF MEMSs, and RF PIN diodes are among the commonly used components for this approach. Although MEMSs and varactors have high Q factors and low insertion losses, their manufacturing processes tend to be more complex and expensive. The chosen solution involves RF PIN diodes, which are relatively inexpensive, easily integrable into circuits, and provide excellent switching. Depending on different switching conditions, the designed antenna can operate in wideband and multiband configurations [31]. Thus, the antenna design can be applied in various frequency bands at a low cost [32, 33].

This paper proposes two new antenna designs. The first is a miniaturized patch antenna which provides good characteristics regarding ultra-broadband, gain, and radiation. On the other hand, there is a frequency-reconfigurable patch antenna with two PIN diodes, allowing two ON-OFF switching modes and thus four operation modes characterized by different resonant frequencies and bandwidths. This frequency reconfigurable antenna can be effectively used in many applications ranging from 5G (IEEE 802.15.3), New 6G band (USA 7.125 GHz to 8.40 GHz), WLAN (IEEE 802.11), HiperLAN (IEEE 802.11 a), V2X (IEEE 802.11 p), WiMAX (IEEE 802.166), Wi-Fi 6E (IEEE 802.11 ax), Wi-Fi 7 (IEEE 802.11 be), New Wi-Fi 8(IEEE 802.11bn), S-Band (from 2 GHz to 4 GHz), C-Band (from 4 GHz to 8 GHz), X-Band (from 8 GHz to 12 GHz) and Ku-Band (from 12 GHz to 18 GHz). It is very small in size, and therefore, it is well-suited for small wireless devices. Good simulation results were obtained concerning the reflection coefficient, radiation pattern, and gain of the proposed antenna in multiple frequency bands.

This paper is organized as follows. Section 1 contains the introductory material along with the motivation of this work. Section 2 concentrates on the diamond-shaped patch antenna, covering design methodology, parameter studies, and experimental results. Section 3 describes the reconfigurable patch antenna, including design, switch arrangements, and mode dependence.

2. DIAMOND SHAPE ANTENNA

2.1. Antenna Design Methodology

The proposed patch antenna design uses an FR-4 Epoxy substrate, a common material choice for antenna construction due to its good combination of low cost and mechanical strength, along with a high dielectric constant. This substrate has a relative permittivity ε_r of 4.4, which plays a crucial role in determining the antenna's bandwidth and resonant frequency. On the other hand, there is also a loss tangent of 0.035 for this material, which highlights a certain number of dielectric losses. The actual thickness chosen for the substrate material is 1.6 mm (H_S). Substrate dimension specifications include a length of 20 mm, a width of 20 mm, and a thickness of 1.6 mm, providing an effective base structure for the radiation component. Ground plane and radiating patch materials are copper, which has outstanding electrical conductivity and reliability. Copper layers have a thickness of 0.035 mm, considered a standard thickness for printed circuit board (PCB) design, which provides adequate current flow without any power loss. The combined effects of substrate characteristics, copper thickness, and antenna design determine important parameters such as impedance matching, bandwidth, gain, and radiation efficiency. In view of the antenna's small size, $20 \times 20 \times 1.6\,\text{mm}^3$

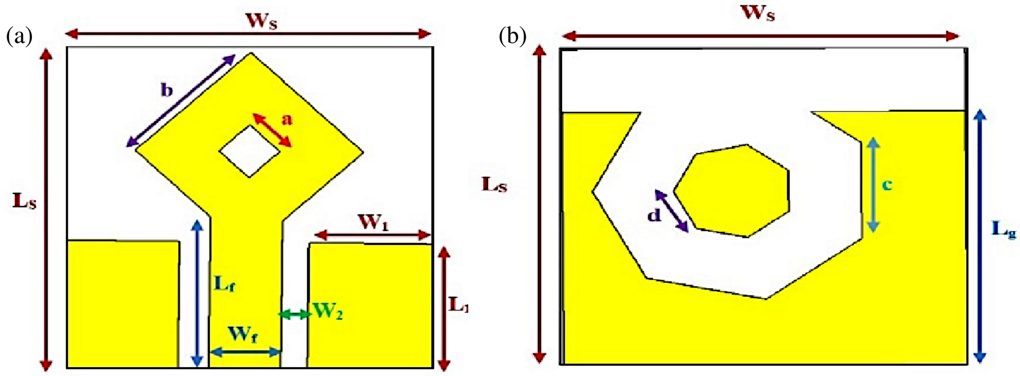

FIGURE 1. Diamond antenna: (a) top view and (b) back view.

, it will be able to work in different frequency bands and hence useful in various applications, such as 5G, New 6G band, WLAN, HiperLAN, V2X, WiMAX, Wi-Fi 6E/7/8, S-, C-, X- and Ku-bands. Apart from being useful in wireless communications, this type of antenna will also find other applications due to its multi-frequency capabilities, which might include new 6G standard applications. In addition to using the antennas in various frequencies, this antenna is also versatile and can be used in future wireless communications, including telephone, sensor networking, and portable devices operating at high speeds on 5G sub-6 GHz and sub-7 GHz.

To present a proper insight into the antenna's design and dimension details, Table 1 lists optimized parameters from the device's electromagnetic simulation and experimentation. The parameters include patch and slot size, feed location, and ground plane modification designed to improve ultra-wideband operation and antenna efficiency. In addition, Fig. 1 highlights the antenna's graphical presentations viewed from its top and rear views. The illustration shows the design and geometry of the patch and ground plane in its base form without any reconfiguration elements.

TABLE 1. Antenna's dimension values.

Parameters	W_s	L_s	W_1	L_1	W_f	L_f
Values (mm)	20	20	6.8	8	3.8	9.6
Parameters	a	b	c	d	L_g	W_2
Values (mm)	1.6	6	6	2.5	16	3

This fundamental design method, based on thoroughly studied substrate and conductor materials, creates a strong foundation for realizing desired broadband capabilities and miniaturization, which are crucial for future wireless communication technologies.

In the present design, the antenna is fed using a waveguide port to optimize power transfer from the feeding source to the radiating element. An impedance transformer is used between the feeding point and the antenna in order to minimize reflections and match impedance levels. There are two major influences on the antenna's electromagnetic behavior with regard to changes introduced into its geometry: the influence of DGS parameters and that of slots introduced into the patch. This happens because changes in the aforementioned geometrical features alter the current distribution inside the antenna, which in turn changes the antenna's electrical lengths and allows one to tune its operating frequencies.

The performance validation of the presented design was conducted using full-wave simulations, and the obtained results were thoroughly examined. Performance parameters such as reflection coefficient S_{11}, gain, and directivity were carefully selected and analyzed to provide insight into the antenna performance under investigation in terms of its characteristics within the specified frequency ranges. The results for the reflection coefficient show that the impedance matching is achieved successfully, and gain and directivity indicate that the designed antenna is suitable for modern wireless applications.

Fig. 2 shows the simulated S_{11} of the optimum antenna with optimized parameters.

The design procedure of the rectangular microstrip patch antenna follows classical expressions described in [34]:

$$L_f = \frac{v_0}{2f_r\sqrt{\varepsilon_{reff}}} - 2\Delta L\,(1) \tag{1}$$

$$W_f = \frac{v_0}{2f_r}\sqrt{\frac{2}{\varepsilon_r+1}} \tag{2}$$

where v_0 is the free space velocity of the light, and f_r is the resonant frequency.

The above model considers the rectangular patch antenna an array of two slots, each of width W and height h and spaced apart by a distance L. Electrically, the length L is increased by ΔL on either side due to the fringing effect [35], with:

$$\Delta L = 0.412h\frac{(\varepsilon_{reff}+0.3)(\frac{W}{h}+0.264)}{(\varepsilon_{reff}-0.258)(\frac{W}{h}+0.8)} \tag{3}$$

The effective dielectric constant is calculated using the formula:

$$\varepsilon_{reff} = \frac{\varepsilon_r+1}{2} + \frac{\varepsilon_r-1}{2}\left[1+10\frac{h}{W}\right]^{-\frac{1}{2}} \tag{4}$$

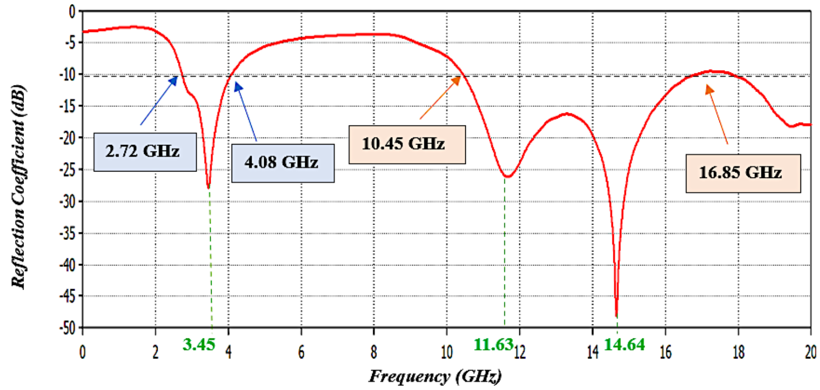

FIGURE 2. The antenna's reflection coefficient.

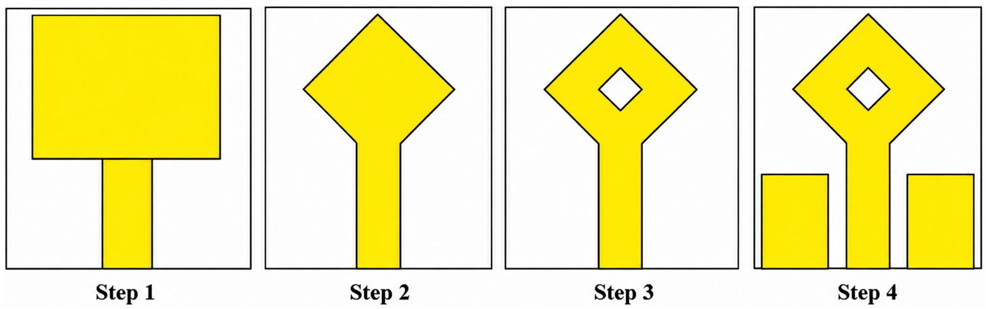

FIGURE 3. Diamond antenna's design steps.

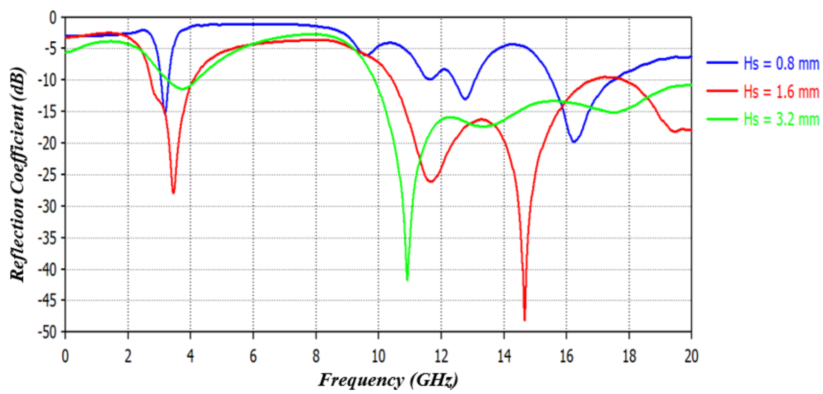

FIGURE 4. The S_{11} for different substrate's thicknesses.

The transmission line model works only for infinite ground planes, but in practice, it is necessary to consider a finite ground plane [11]. Parameters of the ground plane are defined by the following two equations:

$$L_g = L + 6h \quad (5)$$

$$W_g = W + 6h \quad (6)$$

To show the effect of different parameters and study how geometric variations influence the reflection coefficient, Fig. 3 depicts the four-step intelligent design process of the proposed antenna carefully crafted to use the antenna's physical size and resonance properties. First of all, a simple rectangular radiating element is studied in Step 1. Then, Step 2 shows how the rectangle can be turned through an angle of 45° into a diamond-shaped patch and how this change significantly influences the surface current distribution. In particular, such a rotation increases the electrical length of surface currents by a factor of about $\sqrt{2}$. Therefore, this patch's fundamental resonant frequency is reduced by 29%, which allows the antenna's significant miniaturization. Step 3 involves cutting out a central square cut-out to control the input impedance via this structural subtraction, which introduces a built-in reactive element, whereby the internal fringing fields help introduce a shunt capacitance that compensates for the patch inductance. Not only does this step lower the primary resonance, but it also introduces a second resonance point at 11.63 GHz. In Step 4, side

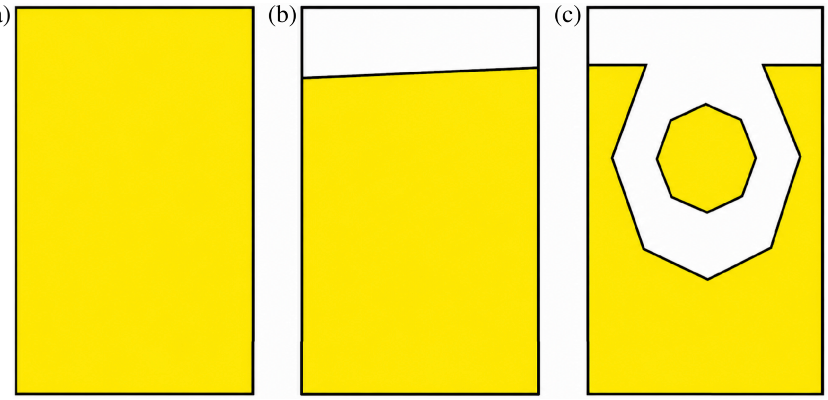

FIGURE 5. The ground plane's steps.

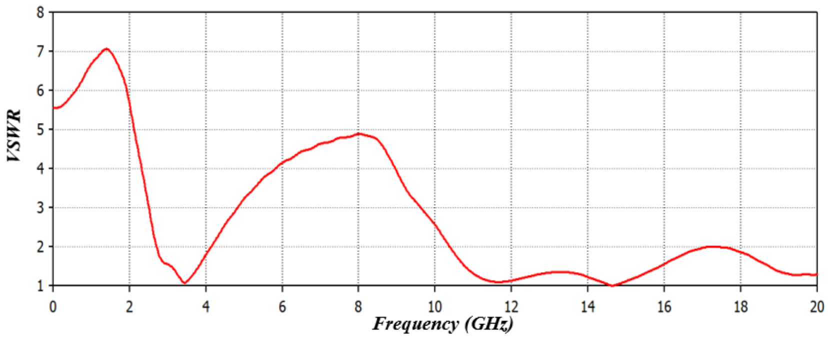

FIGURE 6. Simulated VSWR of the suggested antenna.

partial grounds are added to introduce the coplanar waveguide (CPW) transition.

Substrate thickness selection is very important for the overall characteristics of the proposed antenna. As can be seen from the parametric analysis in Fig. 4, changing the substrate height results in significant differences in resonant frequencies and impedance matching. In general, increasing the substrate thickness leads to improving the impedance bandwidth, but at the same time, this parameter stimulates the formation of surface waves that decrease radiation efficiency and distort the radiation pattern. In contrast, a thin substrate prevents surface waves but limits the available bandwidth and changes the coupling capacitance. Hence, a height of 1.6 mm was selected as an optimal parameter. It ensures good impedance matching in all required frequency bands, improves available bandwidth, and prevents surface waves.

Fig. 5 shows the design of the antenna's ground plane. The progression of the ground plane structure occurs in three steps. Initially, a conventional ground plane with full copper results in reducing the resonant path length and impedance bandwidth since the ground plane has a closed boundary. To circumvent this challenge, the structure's top part is truncated, forming a partial ground plane that creates a diffractive edge effect. The ground plane becomes a radiative aperture in the process, whereby the length of the partial ground plane L_g becomes an independent matching parameter. Finally, introducing a heptagonal Defected Ground Structure (DGS) with an inner conductor on the partial ground plane enhances impedance bandwidth. Including the DGS slot increases the current flow length by forcing the current to go around the slot region, thus lowering the resonant frequency. In addition, the inner conductor causes Complementary Split-Ring Resonator (CSRR)-type shunt resonances, leading to reduced resonant frequency.

The literature states that good antenna performance can be measured in Voltage Standing Wave Ratio (VSWR), which should be below 2 [35]. As shown in Fig. 6, a VSWR ratio of less than 2 suggests good impedance matching between the antenna and the feed network [34]. The condition for VSWR lower than 2 is when less than 10% of the input power is reflected, with 90% going to the antenna. This result indicates that there is optimal antenna efficiency in transmitting power, making the result impressive and proving that the antenna performance is good in terms of effectiveness.

2.2. Parametric Study

In this study, we have studied the effect of changes in the substrate's length and width. These parameters affect the resonance frequency and coupling between the antenna and ground. Thus, there is a decrease in the reflection coefficient, which indicates better impedance matching. Figs. 7 and 8 show the effects of both substrate dimensions. In Fig. 7, W_s is varied from 18 mm to 22 mm. In the figure, the reflection coefficient improves as the width varies. The optimum width of 20 mm gives the best results in terms of impedance matching. In the same manner, in Fig. 10, the substrate length, L_s, is changed from

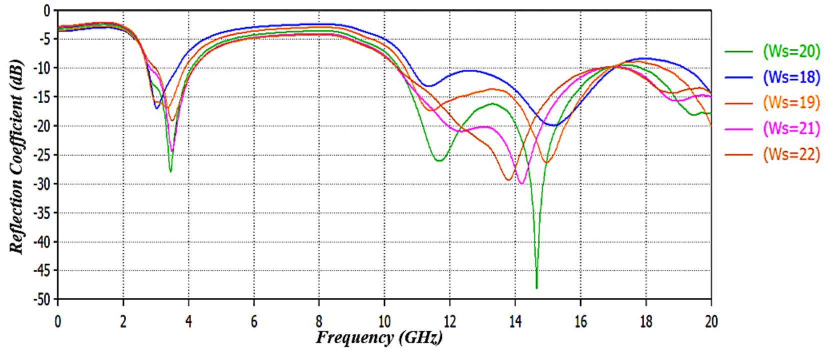

FIGURE 7. The S_{11} variation as function of W_S.

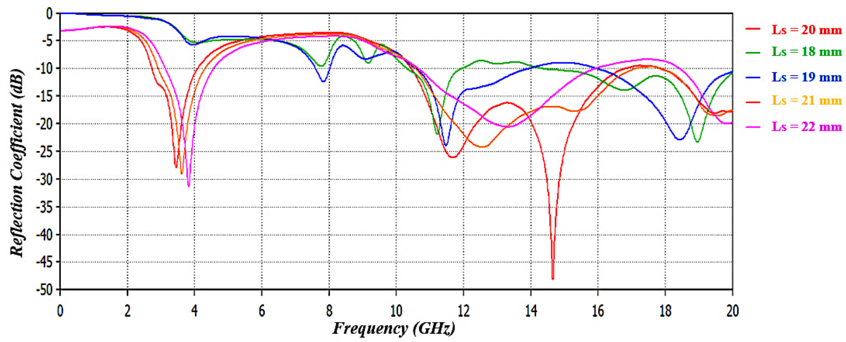

FIGURE 8. The S_{11} variation as function of L_S.

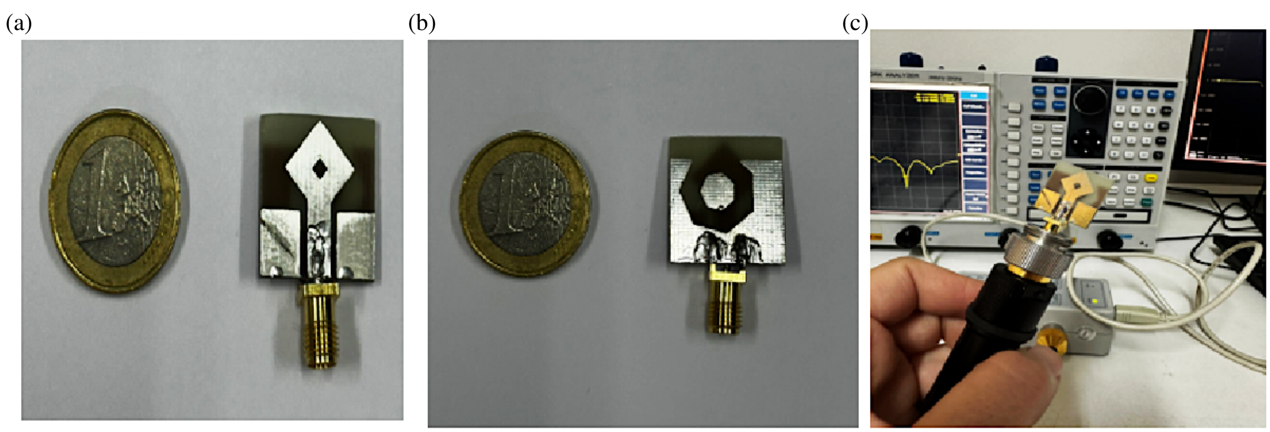

FIGURE 9. Construction prototype: (a) top view, (b) bottom view, and (c) antenna with VNA.

18 mm to 22 mm. It can be observed that 20 mm provides the optimum value for the reflection coefficient.

3. SIMULATED & MEASURED RESULTS AND DISCUSSION

A Ceyear VNA (model 3656D) was used to determine the antenna's S-parameters. Figs. 9 and 10 illustrate the antenna's prototype design under consideration and obtained measurement data, respectively. From the figures above, graphs for VSWR and reflection coefficient agree well with modeled values. However, there are a few discrepancies that need to be mentioned, such as noisy VSWR measurements and minor changes in reflection coefficient values at resonant points. These errors are due to issues with the soldering process for the feed line and ground plane. The interference caused by waves moving through the antenna's radiation pattern also plays a role.

Fig. 11 shows surface current distributions at the three resonant frequencies. Before activating the PIN diode, all segment gaps are kept open, and the multiband behavior is due to the effect of the passive configuration, namely, the heptagonal DGS and the square slot cut in the diamond-shaped patch.

At 3.45 GHz, a strong surface current is concentrated along the feedline wall. Since current cannot pass through the heptagonal DGS slot, the current flows around the slot's edges to increase its electrical length and shift the resonant frequency

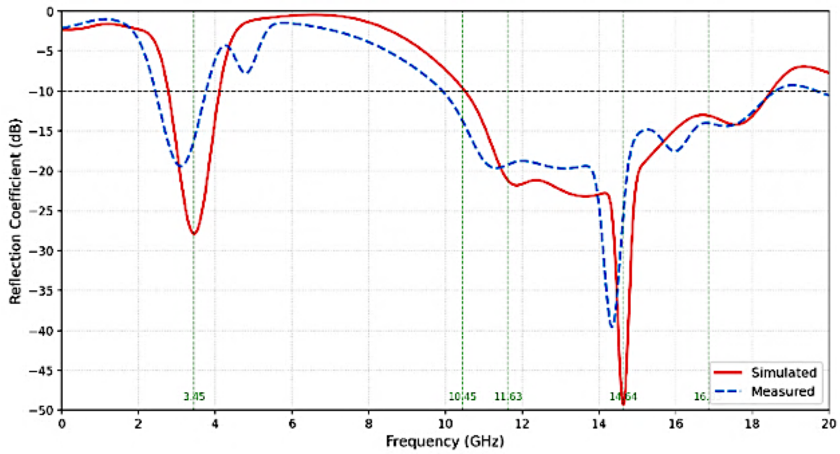

FIGURE 10. Simulated & measured results for S_{11}.

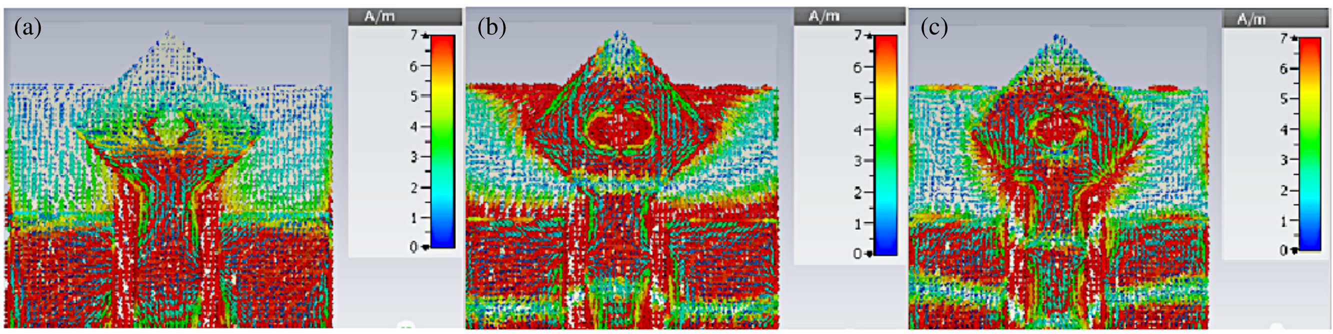

FIGURE 11. Distributions of surface current at (a) 3.45 GHz, (b) 11.63 GHz, and (c) 14.64 GHz.

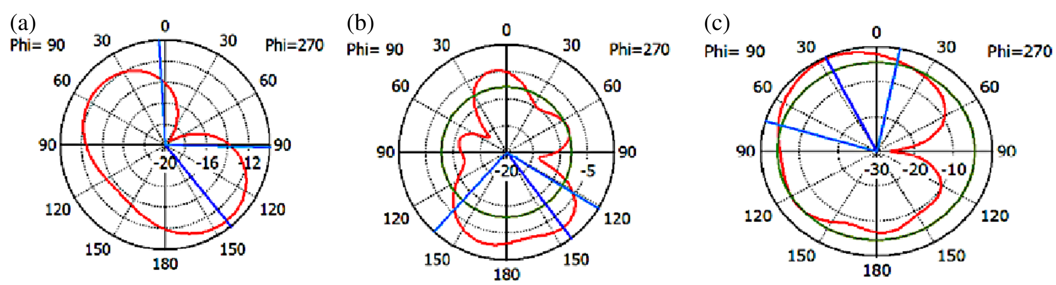

FIGURE 12. Two-dimensional radiation characteristics (H-Plane) at (a) 3.45 GHz, (b) 11.63 GHz, and (c) 14.64 GHz.

below that which could be obtained using only the patch size. At 11.63 GHz, the new maximum location shifts to the perimeter of the slot square. Closed-loop current vectors rotate about all four sides of the slot square and display a symmetrical property with respect to the vertical feed axis, which suggests the slot's even-mode resonance, with the characteristic length equal to one-half the slot perimeter. A higher-order mode is created due to electromagnetic interaction between the mode associated with the rotated square patch, which is known as a corner dipole mode, and a higher-order mode that exists within the heptagon-shaped defected' grounded structure resonator. The current intensity is high at the four corners of the rotated square patch, whereas the center region has medium current intensity. Figs. 12 and 13 illustrate the radiation characteristics of resonant frequencies.

From the analysis of radiation patterns, the following fundamental conclusions about the antenna's passive electromagnetic characteristics can be made:

Gain vs. Modal Relationship: The gain variation is directly related to the surface-current distribution on the patch antenna. The minimum gain, observed at the resonant frequency 3.45 GHz (approximately −12 dB), is attributed to the dominant surface currents flowing on the ground plane, resulting in very low radiation resistance. In contrast, the maximum gain (approximately −1 dB) occurs when the antenna operates in the 11.63 GHz slot mode, as shown in Fig. 14.

Decoupling Spectral and Spatial: The different development stages of the far-field pattern, going through the quasi-omnidirectional (3.45 GHz) to the squinted (11.63 GHz) and then to the multi-lobe (14.64 GHz) pattern, demonstrate that

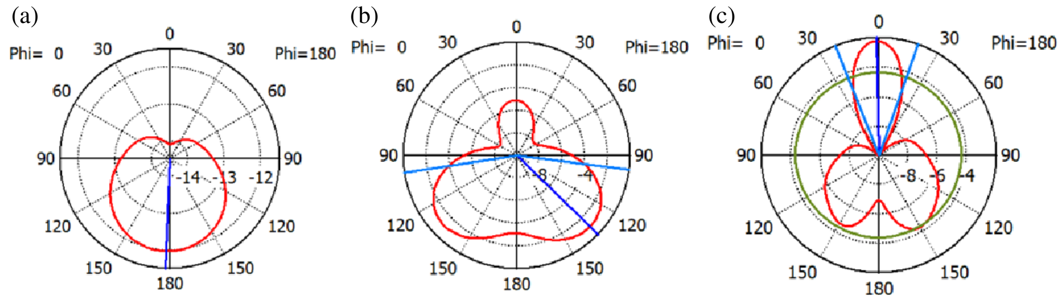

FIGURE 13. Two-dimensional radiation characteristics (E-Plane) at (a) 3.45 GHz, (b) 11.63 GHz, and (c) 14.64 GHz.

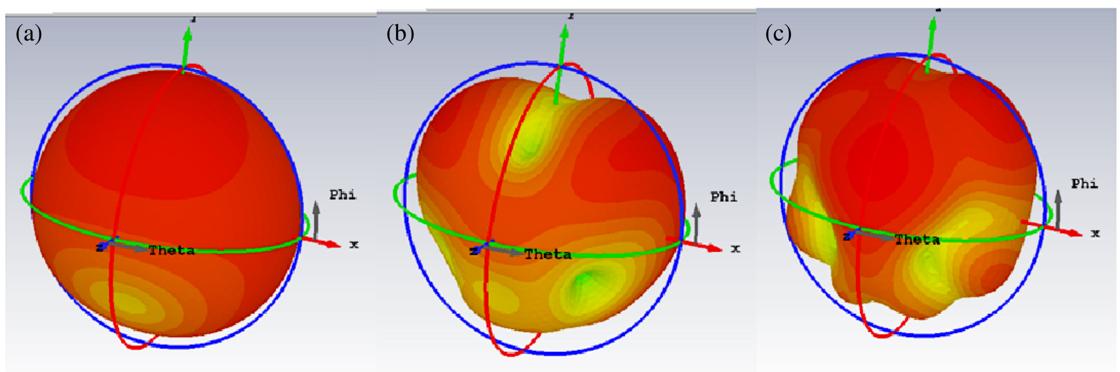

FIGURE 14. Three-dimensional radiation characteristics at resonant frequencies.

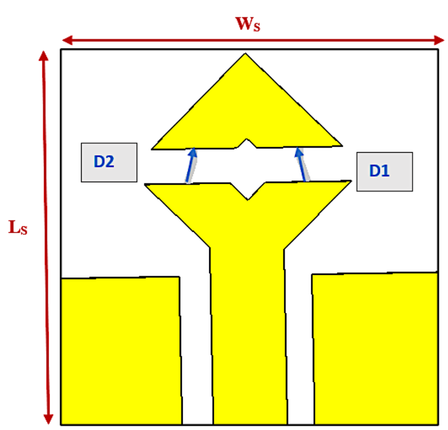

FIGURE 15. Frequency-reconfigurable antenna structure.

each of these frequencies does not simply represent another spectral shift in the same configuration of the geometry of the current. This is an important precondition for the active reconfiguration of the resonant frequency since it ensures that each PIN diode will selectively block a given radiating mode.

Appropriateness to Target Applications: While the occurrence of back-hemisphere radiation within both lower and higher frequency ranges is not ideal for point-to-point communication links, there is a marked benefit provided by this particular form of radiation when being applied to certain network architectures. Specifically, this is beneficial for IoT sensors and 5G-NR user terminals.

4. RECONFIGURABLE ANTENNA

4.1. Antenna Design Methodology

Reconfigurable antennas are those that possess any one feature that can be modified following their manufacturing process. Reconfigurable antennas can modify parameters such as frequency range, impedance, radiation patterns, and polarization so as to adapt themselves according to the environment. The basic antenna architecture does not change; rather, they become reconfigurable via mechanical or electrical means.

Various switching methods, such as RF MEMSs, PIN diodes, FETs, and varactor diodes, have helped antenna reconfigurations. They are evaluated in Table 2. For the new method, we chose PIN diodes because they switch quickly, do not cost an arm and a leg, and are easy to integrate into planar microstrip layouts.

This section describes the suggested antenna design in detail, with the front view shown in Fig. 15. To attain frequency reconfigurability, PIN diodes have been used in the antenna design, and such diodes are ideal for this purpose because of their small size, quick response time, and reliability.

Figure 16 shows a simplified RLC model, which is equivalent to the PIN diode. In order to simulate the behavior of the PIN diode, the PIN diode can be replaced with this simplified model based on the information provided by the manufacturer. The value of inductance, L, is 0.15 nH for both OFF and ON cases. As the PIN diode turns ON, the simplified model can be drawn using a series connection between the resistor 4.7 Ω and L inductance. Similarly, for the deactivated case of the PIN diode, the simplified model consists of two parallel com-

TABLE 2. Characteristics of RF switching elements.

Parameter	Varactor	PIN Diode	MEMS	FET
Voltage (V)	0.1–15	3–5	20–100	3–5
Current (mA)	1–25	3–20	0	0–10
Power (mW)	10–200	5–100	0.05–0.1	0.05–300
Speed (s)	10^{-6}	10^{-6}	10^{-5}	10^{-9}
Sensitivity	Elevated	Moderate	Reduced	Moderate
Cost	Reduced	Very Limited	Elevated	Reduced
Complexity	Minimal	None	Reduced	None

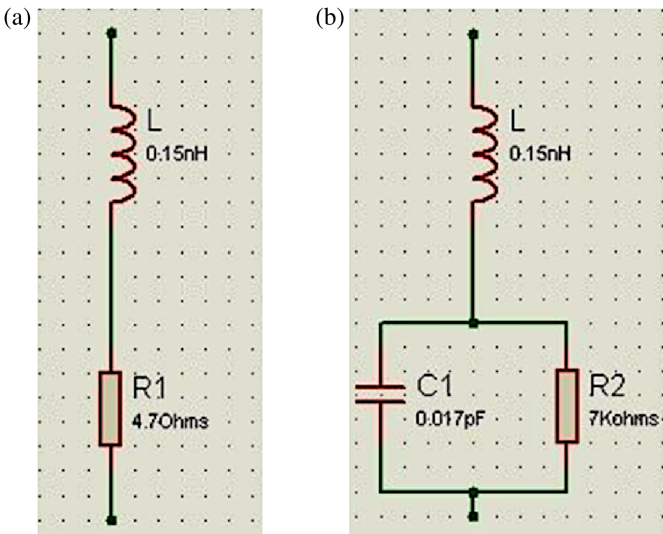

FIGURE 16. Equivalent lumped-element models for PIN diode: (a) ON (forward-biased) state and (b) OFF (reverse-biased) state.

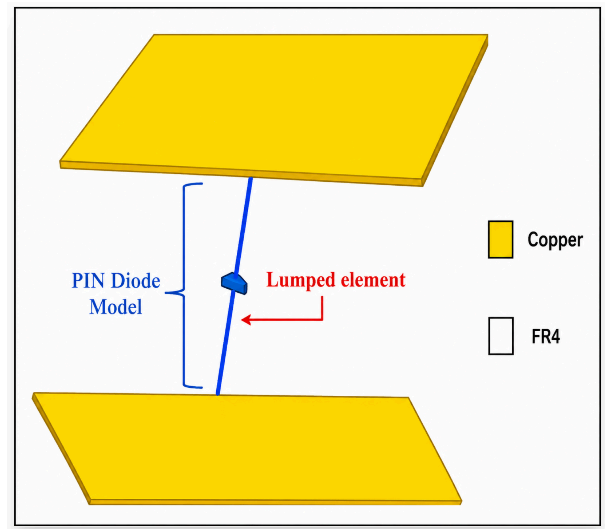

FIGURE 17. Modeling PIN diode behavior in CST MWS.

ponents: a 0.017 pF capacitor and a 7 kΩ resistor, along with L inductance.

The simulation software used for modeling the PIN diode through lumped-element models is Computer Simulation Technology (CST) Microwave Studio (MWS), which provides a suitable option for the proposed design, as suggested in [36] and shown in Fig. 17. Two PIN diodes are used in order to provide the ability to configure the frequency of the proposed reconfigurable antennas, as shown in Fig. 15. Both PIN diodes may be in ON or OFF states, hence four different operation modes.

To develop a frequency-reconfigurable antenna that fulfills the needs of 5G, Upcoming 6G, WLAN, WiMAX, C-, X-band, LTE, V2X, Wi-Fi 6E/7/8 applications, diode placements have been optimized.

4.2. Performance Evaluation Through Simulation

By dynamically altering surface-current paths, S_{11} characteristics demonstrate that complete frequency reconfigurability can be achieved across the four PIN-diode biasing states. Table 3 summarizes all antenna operating modes and their corresponding frequencies. The first state, namely All ON mode, creates an unbroken conductive boundary, creating the fundamental frequency at 3.5 GHz, along with other resonance modes that extend up to 15.2 GHz and are used for Sub-6 and Ku-bands. In contrast, All OFF mode separates all the segments resulting in a fundamental resonance of 4.4 GHz for 5G C-band operation. Importantly, the asymmetric design of single ON modes results in a very high path length for currents, creating non-symmetry in electromagnetic-energy distribution and thus the lowest fundamental resonances (2.6 GHz and 2.9 GHz) for LTE, Wi-Fi 6E/7/8, and sub-6 GHz IoT bands, as shown in Fig. 18.

The key distinguishing feature of the Mode 1 switching state, compared with the unloaded baseline, is not the additional number of resonances, but their physical origin as presented in Fig. 19. For the baseline configuration, the resonances originate only from the antenna geometry. In Mode 1, the topological change introduced by the ON-state diodes, which merges the arc, creates two additional resonances (8.34 and 10.81 GHz) that do not exist in the corresponding passive structure and perturbs the existing resonance at 3.45 GHz to 3.5 GHz. Finally, the 15.17 GHz resonance can be attributed to capacitive coupling between gaps, which becomes stronger with increasing frequency.

Based on Mode 1's far-field investigation, as shown in Figs. 20 and 21, it can be concluded that 8.34 GHz is the optimal operating frequency for directional antenna performance, as it provides excellent broadside radiation with a front-to-rear ratio of approximately 10–12 dB. On the other hand, the secondary resonant frequencies (3.5, 10.81, and 15.17 GHz), despite having beam tilting and multiple-lobe radiation resulting

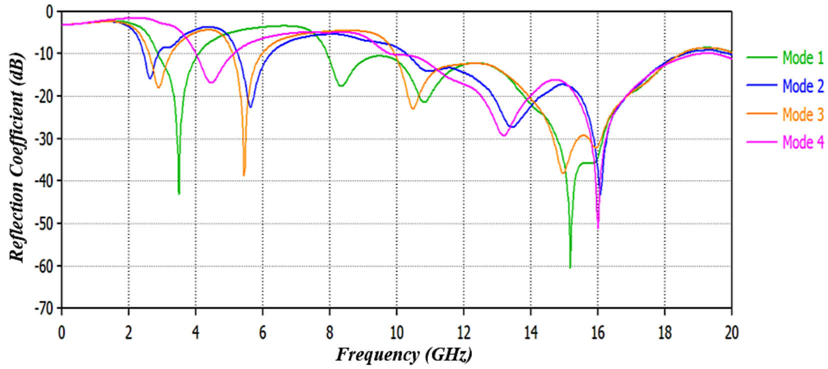

FIGURE 18. The S_{11} of the reconfigurable antenna in all modes.

TABLE 3. Modes of operation for the suggested reconfigurable antenna.

Mode	State of Diodes	Resonant Frequencies (GHz)	Operational Band (GHz)	Target Application Area
Mode 1	D1 & D2 ON	3.5	2.87–4.08	Sub-6 GHz 5G NR (n77/n78), WiMAX, S-band IoT links
		8.34	7.93–18.5	X-/Ku-band satellite links, radar, wideband backhaul; 6G FR3 candidate band (7–24 GHz)
		10.81		
		15.17		
Mode 2	D1 ON & D2 OFF	2.6	2.45–2.86	ISM band, Wi-Fi 6E/7/8, WiMAX, Bluetooth/Zigbee IoT sensors
		5.64	5.25–6.23	WLAN 5 GHz (802.11a/n/ac), Wi-Fi 6E/7/8, 5G NR n79
		13.44	10.27–18.64	X-/Ku-band satellite and radar applications, 6G FR3 candidate band (7–24 GHz)
		16.08		
Mode 3	D1 OFF & D2 ON	2.9	2.6–3.25	Sub-6 GHz 5G NR (n77/n78), WiMAX
		5.44	5.1–5.98	WLAN 5 GHz, C-band applications, Wi-Fi 6E/7/8
		10.48	9.93–18.48	X-/Ku-band satellite and radar applications, 6G FR3 candidate band (7–24 GHz)
		14.98		
		15.96		
Mode 4	D1 & D2 OFF	4.48	4–5.12	C-band wireless links, WLAN 5 GHz
		13.2	9.78–19.1	X-/Ku-band satellite and radar applications; 6G FR3 candidate band (7–24 GHz)
		16		

from phase imbalance and parasitic interaction, provide an essential advantage in IoT networks and 5G NR UE applications due to quasi-omnidirectional spatial coverage.

In summary, the results from the electromagnetic simulations validate the highly versatile multi-band performance of the suggested architecture in its four unique switching modes. Introducing PIN diodes in the suggested architecture enables accurate and precise tunability of the resonance frequency and the bandwidth, while maintaining optimized impedance matching. Therefore, the suggested antenna is able to handle a wide range of wireless systems' standards, including LTE, Wi-Fi 7/8 WLAN, WiMAX, 5G, C-band, X-band, and Ku-band operations. In other words, superior performance characteristics make this antenna an attractive candidate in 6G wireless communication technology.

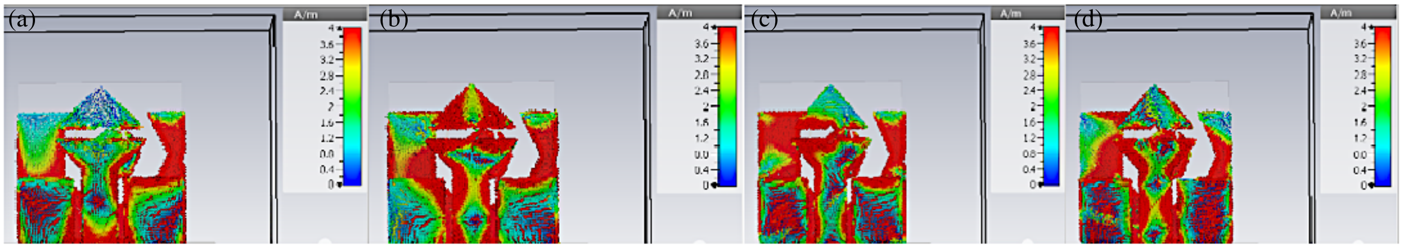

FIGURE 19. Distributions of surface current in mode 1. (a) 3.5 GHz, (b) 8.34 GHz, (c) 10.81 GHz, and (d) 15.17 GHz.

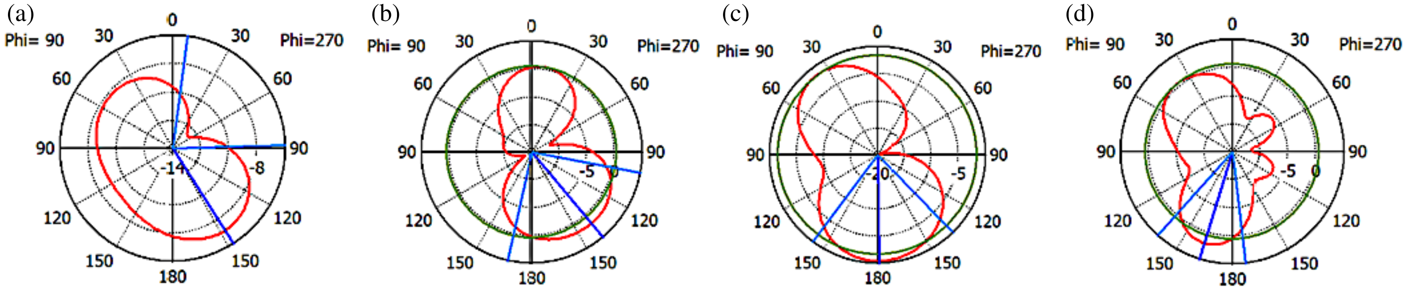

FIGURE 20. Two-dimensional radiation characteristics (H-Plane) in mode 1. (a) 3.5 GHz, (b) 8.34 GHz, (c) 10.81 GHz, and (d) 15.17 GHz.

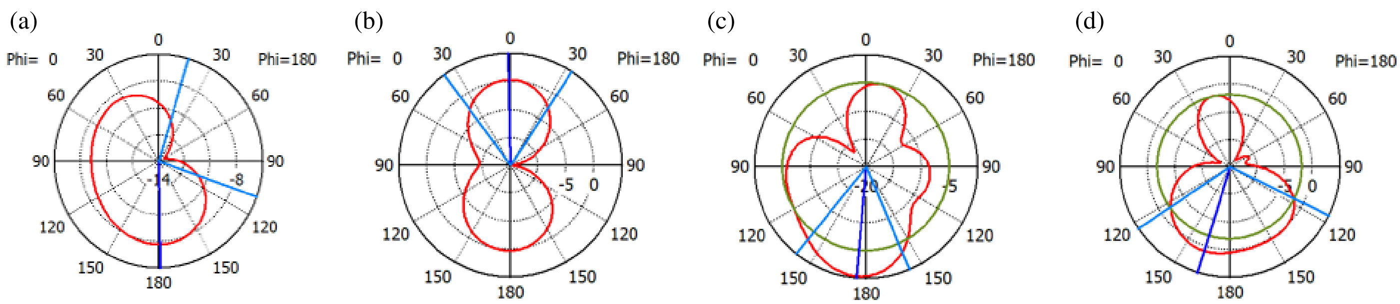

FIGURE 21. Two-dimensional radiation characteristics (E-Plane) in mode 1. (a) 3.5 GHz, (b) 8.34 GHz, (c) 10.81 GHz, and (d) 15.17 GHz.

TABLE 4. Benchmarking with recent works.

Ref.	Dim (mm^2)	N° of operating bands	Bandwidth (MHz)	N° of Switches	Gain (dB)
[27]	40 × 37.2	2	500 & 630	4	0.65 & 1.92
[37]	45 × 50	1	800	2	2.2
[38]	112 × 52	2	1400 & 1501	18	3.8 & 8.3
[39]	113 × 113	2	-	14	6.2 & 6.6
This Work	20 × 20	10	1170 & 10500 & 420 & 950 & 8250 & 670 & 860 & 8630 & 1110 & 911	4	Peak Gain = 2

Although the basic diamond-slot radiator has been successfully manufactured and analyzed to prove the basic design principle, one drawback of the present work is that the PIN-diode reconfigurable antenna has been tested by only simulations using CST Studio Suite. As a result of present-day restrictions in manufacturing technologies, physically testing active states of the reconfigurable antenna has been impossible in this work. Therefore, our next goal in the near future is to manufacture the reconfigurable antenna and test its physical performance in detail.

The performance analysis of the suggested antenna design was done by comparing its performance with those of recently reported antennas with respect to critical design specifications including the number of switches, frequency range, bandwidth, gain, and physical dimensions. Table 4 presents the comparison summary.

It is quite clear from the above data that the proposed design has several merits compared with other designs, including multi-band operation capability and compact dimensions. First, the proposed design can operate at different frequency bands while using a small number of PIN diodes. Other designs, in comparison, use more switches to attain multi-band capability or operate at fewer frequency bands.

5. CONCLUSION

In conclusion, this paper has highlighted the design and electromagnetic performance assessment of a compact, frequency-selective antenna to accommodate the needs of current wireless communication systems. Using the appropriate control of integrated PIN diodes, the design is able to dynamically select different operating frequency bands. Simulation results indicate consistent efficiency around 79%, together with ideal voltage standing wave ratios and impedance matching throughout all targeted bands. Additionally, the antenna exhibits an almost omnidirectional far-field pattern, providing a wide coverage essential for connectivity in modern network systems. Having succeeded in combining spatial reduction with the ability to cover multiple bands, this antenna configuration shows great potential for operation in many different communication protocols, such as LTE, WLAN, WiMAX, Wi-Fi 6/6E/7/8, 5G, and even upcoming 6G networks. Further study will focus on the antenna's actual construction and testing, as well as its validation against simulated parameters. The next stage of the work is also expected to examine the possibility of replacing the currently used PIN diodes with RF MEMSs and varactors, to minimize energy consumption and provide frequency-tuning capability.

ACKNOWLEDGEMENT

The authors express their sincere gratitude to the Ministry of Higher Education (MOHE), Malaysia, Universiti Teknikal Malaysia Melaka (UTeM), under Grant No. PJP/2025/FTKEK/PERSPEKTIF/SA0087, and Asia Pacific University of Technology & Innovation (APU) for their support.

REFERENCES

[1] Al-Gburi, A. J. A., "Do we really need frequency-selective surface and metasurface reflectors for antenna gain enhancement, or are metallic reflectors enough?" *International Journal of Antennas and Propagation*, Vol. 2026, No. 1, 2141943, 2026.

[2] Elabd, R. H., R. E. A. Shehata, and A. J. A. Al-Gburi, "Design process of a four-port fractal MIMO antenna: Boosting isolation and diversity for ultra-wideband and X-band systems," *International Journal of Communication Systems*, Vol. 39, No. 9, e70510, 2026.

[3] Abbaoui, H., S. E. E. Aoud, S. U. Ali, A. Ghammaz, H. Belahrach, and S. Ibnyaich, "Design, analysis and implementation of an optimized cost-effective octagonal patch antenna with UWB characteristics for 5G applications and beyond," *AEU — International Journal of Electronics and Communications*, Vol. 190, 155655, 2025.

[4] Varshney, A., D. N. Gençoğlan, and A. J. A. Al-Gburi, "Design process of a miniaturized reconfigurable antenna for 5G sub-6 GHz and diverse applications," *Journal of Electronic Science and Technology*, Vol. 23, No. 4, 100337, 2025.

[5] Syrytsin, I., R. Rodriguez-Cano, A. Kobaykov, and S. Zhang, "Dual-band transparent metasurface for enhanced performance of 5G mm-Wave and sub-6 GHz mobile phone antennas," *IEEE Antennas and Wireless Propagation Letters*, 1–5, 2026.

[6] Ali, A. H. and J. M. Rasool, "Design of a tri-band reconfigurable antenna using metamaterials for IoT applications," *Open Engineering*, Vol. 15, No. 1, 20240076, 2025.

[7] El Aoud, S. E., H. Abbaoui, O. Benkhadda, S. Attioui, N. E. Assri, S. Ibnyaich, A. Zeroual, M. M. Ismail, and A. J. A. Al-Gburi, "Design of a crescent moon-shaped reconfigurable patch antenna using a PIN diode for 5G sub-6 GHz and multistandard wireless applications," *Progress In Electromagnetics Research B*, Vol. 109, 81–93, 2024.

[8] Al-Gburi, A. J. A., "Nems magnetoelectric antennas: Physics, fabrication, and nanoscale wireless sensing paradigms," *Materials Science in Semiconductor Processing*, Vol. 213, 110832, 2026.

[9] Kiani, N., F. T. Hamedani, and P. Rezaei, "Designing of a circularly polarized reconfigurable graphene-based THz patch antenna with cross-shaped slot," *Optical and Quantum Electronics*, Vol. 55, No. 4, 356, 2023.

[10] Benkhadda, O., M. Saih, A. Reha, S. Ahmad, K. Chaji, H. Singh, and A. J. A. Al-Gburi, "A miniaturized reconfigurable antenna for modern wireless applications with broadband and multi-band capabilities," *Progress In Electromagnetics Research M*, Vol. 127, 93–101, 2024.

[11] Hussain, M., W. A. Awan, M. S. Alzaidi, N. Hussain, E. M. Ali, and F. Falcone, "Metamaterials and their application in the performance enhancement of reconfigurable antennas: A review," *Micromachines*, Vol. 14, No. 2, 349, 2023.

[12] Yahya, M. S., S. Soeung, S. K. A. Rahim, U. Musa, S. S. B. Hashwan, and M. A. Haque, "Machine learning-optimized compact frequency reconfigurable antenna with RSSI enhancement for long-range applications," *IEEE Access*, Vol. 12, 10 970–10 987, 2024.

[13] Ullah, S., I. Elfergani, I. Ahmad, I. U. Din, S. Ullah, W. U. R. Khan, T. Ahmad, U. Habib, C. Zebiri, and J. Rodriguez, "A compact frequency and radiation reconfigurable antenna for 5G and multistandard sub-6 GHz wireless applications," *Wireless Communications and Mobile Computing*, Vol. 2022, No. 1, 4658082, 2022.

[14] Prasanna, R., K. Annaram, and K. Venkatalakshmi, "Reconfigurable tri-band UWB antenna using single winding Balun structure," *Wireless Personal Communications*, Vol. 124, No. 2, 1773–1787, 2022.

[15] Hassan, M. and A. Z. M. T. Islam, "Design of compact open-ended wrench-shaped patch antenna for 5G sub-6 GHz band applications," *Journal of Electronics and Electrical Engineering*, Vol. 4, No. 1, 210–224, 2025.

[16] Al-Gburi, A. J. A., "Coin-sized dual-band millimeter-wave (mmwave) antenna with machine-learning-guided impedance prediction," *Progress In Electromagnetics Research M*, Vol. 136, 1–12, 2025.

[17] Varshney, A., D. N. Gençoğlan, and A. J. A. Al-Gburi, "Design process of a miniaturized reconfigurable antenna for 5G sub-6 GHz and diverse applications," *Journal of Electronic Science and Technology*, Vol. 23, No. 4, 100337, 2025.

[18] Sindhuja, N. M. M., R. Sreelakshmy, O. P. Kumar, and M. Raveendra, "Design of a hilbert curve fractal MIMO slot an-

tenna with enhanced bandwidth and stable radiation patterns for Wi-Fi 7 and Wi-Fi 8 applications using genetic algorithm," *International Journal of Antennas and Propagation*, Vol. 2026, No. 1, 8112380, 2026.

[19] Parasher, R., D. Yadav, and A. Saharia, "Design and analysis of hybrid fractal frequency-band reconfigurable metamaterial antenna for multi-standard wireless applications," *Results in Engineering*, Vol. 26, 104696, 2025.

[20] Gençoğlan, D. N., Ş. Çolak, and M. Palandöken, "Spiral-resonator-based frequency reconfigurable antenna design for sub-6 GHz applications," *Applied Sciences*, Vol. 13, No. 15, 8719, 2023.

[21] Kareem, Q. H. and R. A. Shihab, "Reconfigurable compact quad-port MIMO antennas for sub-6 GHz applications," *Journal of Al-Farabi for Engineering Sciences*, Vol. 2, No. 1, 10, 2023.

[22] Tiwari, A., D. Yadav, P. Sharma, and M. V. Yadav, "Design of wide notched-band circular monopole ultra-wideband reconfigurable antenna using PIN diodes switches," *Progress In Electromagnetics Research C*, Vol. 139, 107–118, 2024.

[23] Sree, M. F. A., M. H. A. Elazeem, and W. Swelam, "Dual band patch antenna based on letter slotted DGS for 5G sub-6 GHz application," *Journal of Physics: Conference Series*, Vol. 2128, No. 1, 012008, Cairo, Egypt, 2021.

[24] Agarwal, S. and M. P. Gupta, "Sub-6 GHz novel C-shaped antenna for 5G application," in *2022 IEEE Microwaves, Antennas, and Propagation Conference (MAPCON)*, 729–732, Bangalore, India, 2022.

[25] Kulkarni, N., R. M. Linus, and N. B. Bahadure, "A small wide-band inverted L-shaped flexible antenna for sub-6 GHz 5G applications," *AEU — International Journal of Electronics and Communications*, Vol. 159, 154479, 2023.

[26] Riaz, S., M. Khan, U. Javed, and X. Zhao, "A miniaturized frequency reconfigurable patch antenna for IoT applications," *Wireless Personal Communications*, Vol. 123, No. 2, 1871–1881, 2022.

[27] Kumar, P., S. Dwari, R. K. Saini, and M. K. Mandal, "Dual-band dual-sense polarization reconfigurable circularly polarized antenna," *IEEE Antennas and Wireless Propagation Letters*, Vol. 18, No. 1, 64–68, 2019.

[28] Moses, A. T. Z. and N. Moses, "Compact self decoupled MIMO antenna pairs covering 3.4–3.6 GHz band for 5G handheld device applications," *AEU — International Journal of Electronics and Communications*, Vol. 141, 153971, 2021.

[29] Vinoth, M., R. Prasanna, M. S. Maharajan, and R. R. Kanna, "Multiband reconfigurable MIMO antenna using fractal geometry and PIN diode switches for next generation wireless networks," *Physica Scripta*, Vol. 100, No. 11, 115509, 2025.

[30] Kakhki, M. B. and P. Rezaei, "Reconfigurable microstrip slot antenna with DGS for UWB applications," *International Journal of Microwave and Wireless Technologies*, Vol. 9, No. 7, 1517–1522, 2017.

[31] Nasrabadi, E. and P. Rezaei, "A novel design of reconfigurable monopole antenna with switchable triple band-rejection for UWB applications," *International Journal of Microwave and Wireless Technologies*, Vol. 8, No. 8, 1223–1229, 2016.

[32] Sravani, K. G., D. Prathyusha, G. R. K. Prasad, C. G. Chand, P. A. Kumar, K. Guha, and K. S. Rao, "Design of reconfigurable antenna by capacitive type RF MEMS switch for 5G applications," *Microsystem Technologies*, Vol. 28, No. 3, 845–853, 2022.

[33] Prasanna, R., P. Saravanan, and S. Rajarajan, "Compact tri-band antenna with double winding structures for 3G/4G/5G base station applications," *Wireless Personal Communications*, Vol. 129, No. 1, 371–386, 2023.

[34] Balanis, C. A., *Antenna Theory: Analysis and Design*, John Wiley & Sons, New York, USA, 2016.

[35] El Aoud, S. E., H. Abbaoui, L. Aguni, Z. E. Ouadi, S. Ibnyaich, A. Ghammaz, A. Zeroual, and H. Belahrach, "Design, optimization and prediction of the performances for a multi-band patch antenna using artificial neural network (ANN)," in *Smart Mobility and Industrial Technologies: The Quality of Life in Sustainable Cities*, 55–64, 2022.

[36] Al-Gburi, A. J. A., "CST vs HFSS: A comparative analysis for antenna and microwave engineering," *International Journal of Antennas and Propagation*, Vol. 2026, No. 1, 2733569, 2026.

[37] Ghaffar, A., X. J. Li, W. A. Awan, A. H. Naqvi, N. Hussain, M. Alibakhshikenari, and E. Limiti, "A flexible and pattern reconfigurable antenna with small dimensions and simple layout for wireless communication systems operating over 1.65–2.51 GHz," *Electronics*, Vol. 10, No. 5, 601, 2021.

[38] Shereen, M. K., M. I. Khattak, and M. Al-Hasan, "A frequency and radiation pattern combo-reconfigurable novel antenna for 5G applications and beyond," *Electronics*, Vol. 9, No. 9, 1372, 2020.

[39] Ismail, M. F., M. K. A. Rahim, M. R. Hamid, H. A. Majid, A. H. Omar, L. O. Nur, and B. S. Nugroho, "Dual-band pattern reconfigurable antenna using electromagnetic band-gap structure," *AEU — International Journal of Electronics and Communications*, Vol. 130, 153571, 2021.